Tungsten (2023) 5:589–597
https://doi.org/10.1007/s42864-023-00212-6

Tungsten
www.springer.com/42864

ORIGINAL PAPER

Interfacial engineering of heterostructured carbon-supported molybdenum cobalt sulfides for efficient overall water splitting

Ming-Yue Ma[1] · Han-Zhi Yu[1] · Li-Ming Deng[1] · Lu-Qi Wang[1] · Shu-Yi Liu[1] · Hui Pan[2] · Jian-Wei Ren[3] · Maxim Yu. Maximov[4] · Feng Hu[1] · Sheng-Jie Peng[1]

Received: 17 November 2022 / Revised: 29 December 2022 / Accepted: 3 January 2023 / Published online: 20 March 2023

Abstract
Constructing hetero-structured catalyst is promising but still challenging to achieve overall water splitting for hydrogen production with high efficiency. Herein, we developed a sulfide-based $MoS_2/Co_{1-x}S$@C hetero-structure for highly efficient electrochemical hydrogen evolution reaction (HER) and oxygen evolution reaction (OER). The carbon derived from the filter paper acts as a conducting carrier to ensure adequate exposure of the active sites guaranteed with improved catalytic stability. The unique hierarchical nano-sheets facilitate the charge and ion transfer by shortening the diffusion path during electro-catalysis. Meanwhile, the robust hetero-interfaces in $MoS_2/Co_{1-x}S$@C can expose rich electrochemical active sites and facilitate the charge transfer, which further cooperates synergistically toward electro-catalytic reactions. Consequently, the optimal $MoS_2/Co_{1-x}S$@C hetero-structures present small over-potentials toward HER (135 mV @ 10 mA·cm^{-2}) and OER (230 mV @ 10 mA·cm^{-2}). The $MoS_2/Co_{1-x}S$@C electrolyzer requires an ultralow voltage of 1.6 V at the current density of 10 mA·cm^{-2} with excellent durability, outperforming the state-of-the-art electro-catalysts. This work sheds light on the design of the hetero-structured catalysts with interfacial engineering toward large-scale water splitting.

Keywords Overall water splitting · Composite · Pyrolysis · Interface regulation · Molybdenum cobalt sulfides

1 Introduction

To mitigate the growing global greenhouse issue, the production of carbon–neutral fuels with zero-polluting feature is highly desired [1, 2], in which hydrogen from renewable electricity represents a promising clean energy source for the sustainable economy and society [3–5]. Electrochemical hydrogen generation is achieved using water electrolysis technique [6, 7], which is dominated by the inefficient hydrogen evolution reaction (HER) and sluggish the oxygen evolution reaction (OER). As these two basic reactions are affected by many factors of catalysts, such as the adsorption of intermediates, reaction kinetics, catalyst stability, etc., the design of efficient catalyst remains a great challenge [8, 9]. Currently, commercial metal-based catalysts have been regarded as state-of-the-art catalysts for water splitting, which can reduce the activation energy and facilitate the reaction process. And yet, the high cost, scarcity, and unsatisfactory durability seriously impede their large-scale applications [10–12]. Therefore, the development of earth-rich, non-precious metal catalysts with bifunctional catalytic activity for both HER and OER is highly urgent.

Tremendous efforts have been made to discover earth-abundant and efficient catalysts in recent years, such as metal sulfides [13–16], phosphides [17–19], selenides [20, 21], and metal–organic framework-based compounds [22], to replace noble metal-based catalysts. Among them, transition metal sulfides have rich active sites and higher electronic conductivity compared with oxides, which play an important role in

✉ Feng Hu
fenghu@nuaa.edu.cn

✉ Sheng-Jie Peng
pengshengjie@nuaa.edu.cn

1 College of Materials Science and Technology, Nanjing University of Aeronautics and Astronautics, Nanjing 210016, China

2 Institute of Applied Physics and Materials Engineering, University of Macau, Macao SAR 519000, China

3 Department of Mechanical Engineering Science, University of Johannesburg, Cnr Kingsway and University Roads, Auckland Park, Johannesburg 2092, South Africa

4 Peter the Great Saint-Petersburg Polytechnic University, 195251 Saint Petersburg, Russia

electrochemical energy storage materials [23–25]. Besides, the introduction of S could further enhance the delocalization of electrons in the catalyst, which can provide efficient electron transfer channel to promote the migration of electrons from metal cations to S. It is well known that layered molybdenum sulfide is a typical HER electro-catalyst, but the molybdenum sulfide itself is severely limited in their electro-catalytic performance as bifunctional hydrolysis electro-catalysts [26–28]. Interfacial engineering is considered as an effective strategy to adjust the electronic structure and improve the activity. The interface engineering could be beneficial to enriching the active sites and promoting the electronic transfer, and thus boost the sluggish water splitting efficiency [29, 30]. Heterojunction materials have attracted extensive attention due to their unique electrocatalytic properties at present [31–33]. Specifically, in the electrochemical reaction process, the charge transfer rate is enhanced due to the synergistic effect of the hetero-structure [34]. At the same time, the hetero-structure can regulate the adsorption and desorption energy of reaction intermediates to improve the catalytic performance [35–38]. In addition, suitable substrate material can not only increase the exposed sites, but also improve the catalyst stability by reducing the aggregation during the electro-catalytic reactions. The carbon derived from the filter paper by the pyrolysis with high surface area and conductivity can serve as an ideal catalyst substrate, which can recycle the filter paper during the synthesis of nano-catalysts avoiding large waste [39]. More importantly, the carbon can inherent the three-dimensional structure of cellulose filter paper with excellent adsorption for metal source in water [29, 40]. Furthermore, the carbon material itself has excellent electrical conductivity, and the three-dimensional (3D) network structure of carbon filter paper provides a substantial framework for the deposition of cobalt and molybdenum composites, which can reduce the irregular deposition of hetero-structures [41]. Therefore, the construction of sulfide heterojunction supported by the derived carbon of filter paper is a reasonable strategy for designing efficient bifunctional catalysts [42].

Herein, a simple adsorption-hydrothermal synthesis strategy was demonstrated to successfully construct MoS_2/$Co_{1-x}S$@C hetero-structured composite to investigate the interfacial electronic effect for overall water splitting. Two-dimensional nano-sheets have a relatively large active area and abundant low coordination edges, resulting in abundant active sites, which are benefit to improving the performance of water splitting. The synergistic effect of the MoS_2/$Co_{1-x}S$ and carbon derived from filter paper could significantly enhance the reaction kinetics and activity for overall water splitting. As predicted, the as-prepared hetero-structure MoS_2/$Co_{1-x}S$@C exhibited only 135 mV and 230 mV for HER and OER at 10 mA·cm^{-2}, respectively. Furthermore, for the two-electrode system, the optimal electrolyzer with MoS_2/$Co_{1-x}S$@C as both cathode and anode achieves a low voltage of 1.60 V at 10 mA·cm^{-2}.

2 Experimental

2.1 Chemical materials

All chemicals were used without further purification. Hexa-ammonium hepta-molybdate tetra-hydrate ($(NH_4)_6Mo_7O_{24}\cdot 4H_2O$), cobalt nitrate hexahydrate ($Co(NO_3)_2\cdot 6H_2O$), sublimation sulfur powder (S, 99.9%), and potassium hydroxide (KOH) were purchased from Macklin, while the filter paper, polyvinylidene fluoride (PVDF, 99%), nafion (5 wt.%), platinum on graphitized carbon (Pt/C, 20 wt.%), and ruthenium oxide (RuO_2) were obtained from Aladdin.

2.2 Synthesis of the electro-catalyst

For the preparation of MoS_2/$Co_{1-x}S$@C, the filter paper was used as sacrificial support and carbon source. Firstly, the commercial filter paper was cut into 2×3 cm^2, sonicated with water and ethanol for 30 min each. And the papers were rinsed and dried under a vacuum at 60 °C. Then 1.455 g of $Co(NO_3)_2\cdot 6H_2O$ and 0.883 g of $(NH_4)_6Mo_7O_{24}\cdot 4H_2O$ were dispersed in 5 mL water and sonicated for 20 min. After the mixed solution turned into a dark red homogeneous solution, the pretreated filter paper was soaked for 2 h and then dried under vacuum. The dried filter paper and 0.3 g of sublimated sulfur powder were placed in downstream and upstream portion of one porcelain boat, respectively, and calcined at 600 °C for 5 h in an Ar atmosphere to obtain hetero-structured MoS_2/$Co_{1-x}S$@C. As a comparison, we prepared a comparative $Co_2Mo_3O_8$/MoO_2@C electro-catalyst by a similar method without adding sublimation sulfur.

2.3 Material characterization

Morphology characterizations of the samples were performed on Regulus 8100 scanning electron microscope and FEI Tecnai G2 F20 microscope. The phase composition and crystal structure were analyzed using the Bruker D8 Advance X-ray diffraction system with Cu–Kα radiation. X-ray photoelectron spectroscopy (XPS) testing was operated to evaluate the chemical states of the samples (ESCALAB 250 system). Raman spectra were acquired on a confocal laser micro-Raman spectrometer (Renishaw in Via) with the exciting wavelength of 514.5 nm.

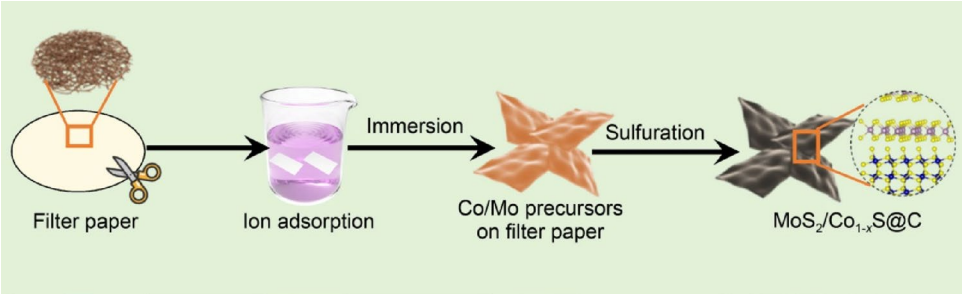

Scheme 1 Schematic illustration for the preparation of $MoS_2/Co_{1-x}S$@C via an adsorption-thermal treatment synthesis

2.4 Electrochemical measurements

The electro-catalytic tests of the samples were carried out on the CS studio equipment. The prepared catalyst, Super P, and binder (PVDF) were mixed in the mass ratio of 7:2:1, ground evenly, and then coated on one piece of nickel foam with an active area of 1×1 cm^2 as the working electrode (WE), Ag/AgCl filled with saturated KCl solution was used as the reference electrode (RE). The carbon rod was used as the counter electrode (CE) for the HER performance test, while the platinum sheet was employed for the OER. All measured potentials are calibrated according to the Nernst equation versus reversible hydrogen electrode (RHE). Activation of the working electrode by cyclic voltammetry was at a scan rate of 50 $mV{\cdot}s^{-1}$ prior to linear sweep voltammetry (LSV). The LSV test was carried out in 1.0 $mol{\cdot}L^{-1}$ KOH at room temperature with a scan rate of 5 $mV{\cdot}s^{-1}$. Electrochemical impedance spectroscopy (EIS) was performed at a frequency from 0.1 to 10^5 with an amplitude of 5 mV.

3 Results and discussion

The brief synthesis of $MoS_2/Co_{1-x}S$@C is shown in Scheme 1. The filter paper is composed of cellulose with polyhydroxy groups, and its higher liquid adsorption is conducive to forming the lamellar stacking of nano-sheets after calcination, improving the electrochemical performance [43, 44]. The filter paper was immersed in a mixture of cobalt and molybdenum salts for ion adsorption, and then the filter paper with adsorbed metal source was calcined at high temperature in an argon atmosphere in the presence of sublimated sulfur to obtain $MoS_2/Co_{1-x}S$@C hetero-structured nano-sheets. Scanning electron microscopy (SEM) images indicate that $MoS_2/Co_{1-x}S$@C has a rough layered structure. Furthermore, the small-sized sulfide particles are uniformly covered and embedded in the carbon fiber matrix, confirming the successful sulfidation of the catalyst (Fig. 1a, b). For comparison, the treated filter papers were soaked in mixed solutions of different concentrations. When the solution concentration is low, it is difficult for grains to nucleate and grow, and the construction of hetero-structures is hindered. While the concentration of the metal salts is too high, the morphology of the filter paper can hardly be seen (Fig. S1). It was observed that the optimized ion adsorption of 5 mmol can favor the formation of heterojunctions and provide plenty of sites for synergistic catalytic activity.

The transmission electron microscopy (TEM) images of $MoS_2/Co_{1-x}S$@C further confirm that the nano-sheet structure coupled with many fine nanoparticles, exhibited a relatively rough surface. The synthesized $MoS_2/Co_{1-x}S$@C maintains the ultrathin nano-sheet structure with a large amount of MoS_2 intercalation grown vertically (Fig. 1c, d). This layered structure with a rough surface not only optimizes mass transfer but also avoids Ostwald ripening of the catalyst during the HER process and therefore improves catalytic activity and stability [45, 46]. There are many gaps in the network structure, which can be used as diffusion and transmission channels between reactants and products in the water electrolysis process. At the same time, this is conducive to the conduction of electrons, so as to enhance the transmission of electrons. High-resolution TEM (HRTEM) images with two distinct lattice fringes clearly show the $Co_{1-x}S$ nanoparticles grown around the interface and the existence of micropores, which can establish a rapid mass transfer channel (Fig. 1e) [47]. The planar spacing of the catalyst lattice fringes was accurately measured to be 0.616 and 0.292 nm, corresponding to the (002) and (100) crystal planes of MoS_2 and (100) of $Co_{1-x}S$, respectively (Fig. 1f). In addition, we can clearly see the interface between heterostructures (Fig. S2). The interface between MoS_2 and $Co_{1-x}S$ exposes more active sites for boosting the catalytic reaction [48, 49]. And the elemental mapping displayed a relatively homogeneous distribution of S, Mo, and Co in the $MoS_2/Co_{1-x}S$@C (Fig. 1g). These results confirm the successful preparation of the hetero-structures with obvious interfaces between MoS_2 and $Co_{1-x}S$ supported by carbon.

The structural information and surface chemical states of the hetero-structures were investigated using X-ray diffraction (XRD), Raman spectroscopy, and XPS. To exclude the possible effect of sulfurization, we significantly prepared the electro-catalyst without sulfurization for comparison. The XRD analysis (Fig. 2a) confirms that MoS_2 and $Co_{1-x}S$ with sharp diffraction peaks are indexed to the standard PDF

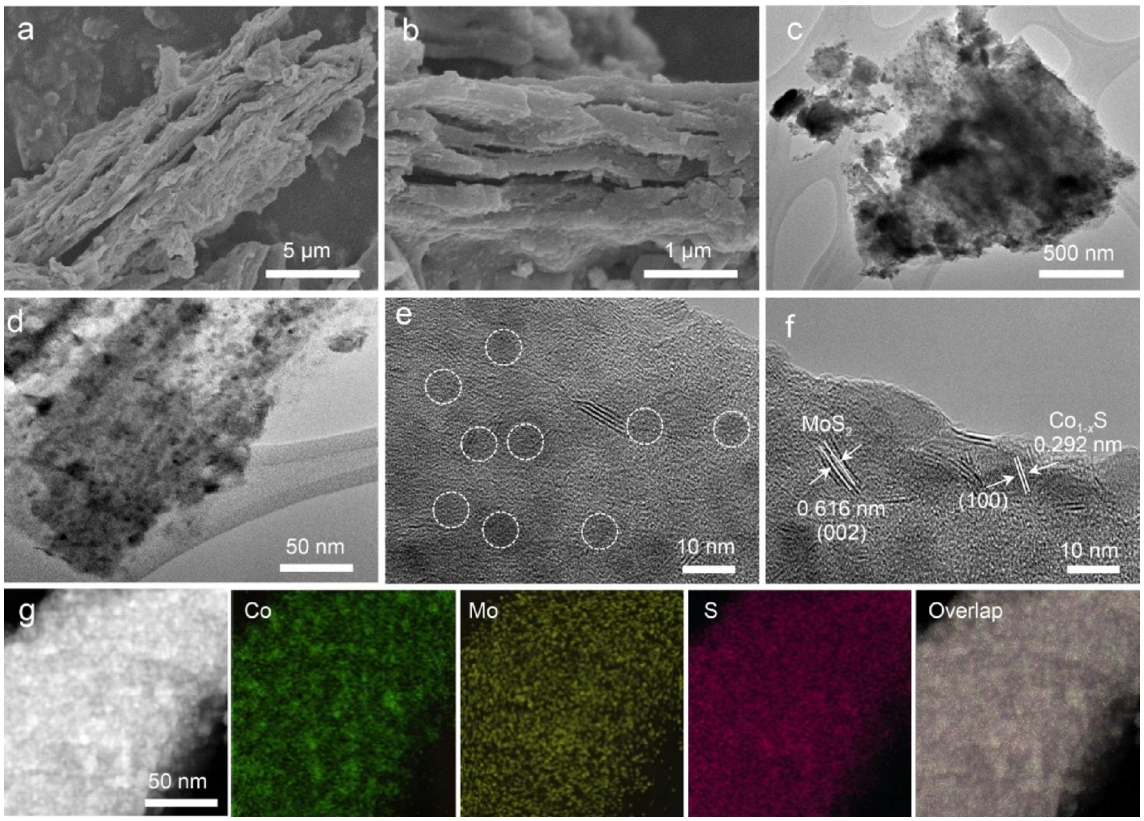

Fig. 1 **a**, **b** SEM images, **c**, **d** TEM and **e**, **f** HRTEM images of $MoS_2/Co_{1-x}S$@C. **g** Elemental mapping reveals the presence and homogenous distribution of Co, Mo, and S elements in $MoS_2/Co_{1-x}S$@C

phase (JCPDF #2–132) and (JCPDF #42–826). By contrast, $Co_2Mo_3O_8/MoO_2$@C corresponds to a main $Co_2Mo_3O_8$ phase and a minor MoO_2 phase (Fig. S3). It is speculated that the carbonization of cellulose has an important effect on the formation of the final substance. Interestingly, no prominent carbon peak was observed in the XRD pattern, which may be due to the amorphous existence form of carbon. The following Raman spectrum further confirms this viewpoint. According to the comparison of Raman results (Fig. S4), the I_G/I_D ratio of $Co_2Mo_3O_8/MoO_2$@C (1.033) is much smaller than that of $MoS_2/Co_{1-x}S$@C (1.416), indicating that $MoS_2/Co_{1-x}S$@C has a higher degree of graphitization due to the effect of sulfurization, which can tune the electron transport ability and obtain outstanding catalytic activity.

XPS was performed to determine the chemical coupling at the MoS_2 and $Co_{1-x}S$ interfaces by comparing the electron configuration on the $Co_2Mo_3O_8/MoO_2$@C surface. Figure 2b displays the XPS spectra of Mo 3d, four peaks at 235.65 eV, 232.39 eV, 230.33 eV, and 228.83 eV are shown in $Co_2Mo_3O_8/MoO_2$@C, which correspond to Mo^{6+} $3d_{3/2}$, Mo^{4+} $3d_{3/2}$, Mo^{6+} $3d_{5/2}$, and Mo^{4+} $3d_{5/2}$, respectively. A slight shift toward a higher binding energy indicates the strong interaction at the material interface and electron transfer from $MoS_2/Co_{1-x}S$@C. In addition, a characteristic peak of S_2^{2-} 2 s appeared at 226.40 eV, indicating the successful synthesis of the sulfide. As shown in Fig. 2c, for $MoS_2/Co_{1-x}S$@C, two peaks located at 781.04 eV and 782.84 eV correspond to the Co^{3+} $2p_{3/2}$ and Co^{2+} $2p_{3/2}$, it is clearly noted that the shift in binding energy to lower values becomes more pronounced for $Co_2Mo_3O_8/MoO_2$@C, manifesting that there is a coupled interface and strong interaction between MoS_2 and $Co_{1-x}S$ [50]. In addition, the S 2p spectrum in Fig. 2d shows the superposition of S_2^{2-} (165.28 eV and 163.28 eV) and S^{2-} (161.91 eV and 160.23 eV). A pair of peaks at 168.77 eV corresponds to sulfate, and the S atom may exist in the apical S^{2-} or bridged S_2^{2-} form, which are active sites for the HER reaction process. Based on the results of the above description, the synthesized $MoS_2/Co_{1-x}S$@C hetero-structured nano-sheets have multi-dimensional cross-linked structure. It has been reported that this structure may provide abundant active sites to accelerate mass/charge transfer, and resulting a superior catalytic activity for overall water splitting [34].

To elucidate the effect of interfacial coupling on catalytic performance of $MoS_2/Co_{1-x}S$@C, the electro-catalytic HER and OER activities were measured in 1.0 mol·L^{-1} KOH by a three-electrode system with $Co_2Mo_3O_8/MoO_2$@C and commercial catalysts as the electrodes. Figure 3a is the LSV

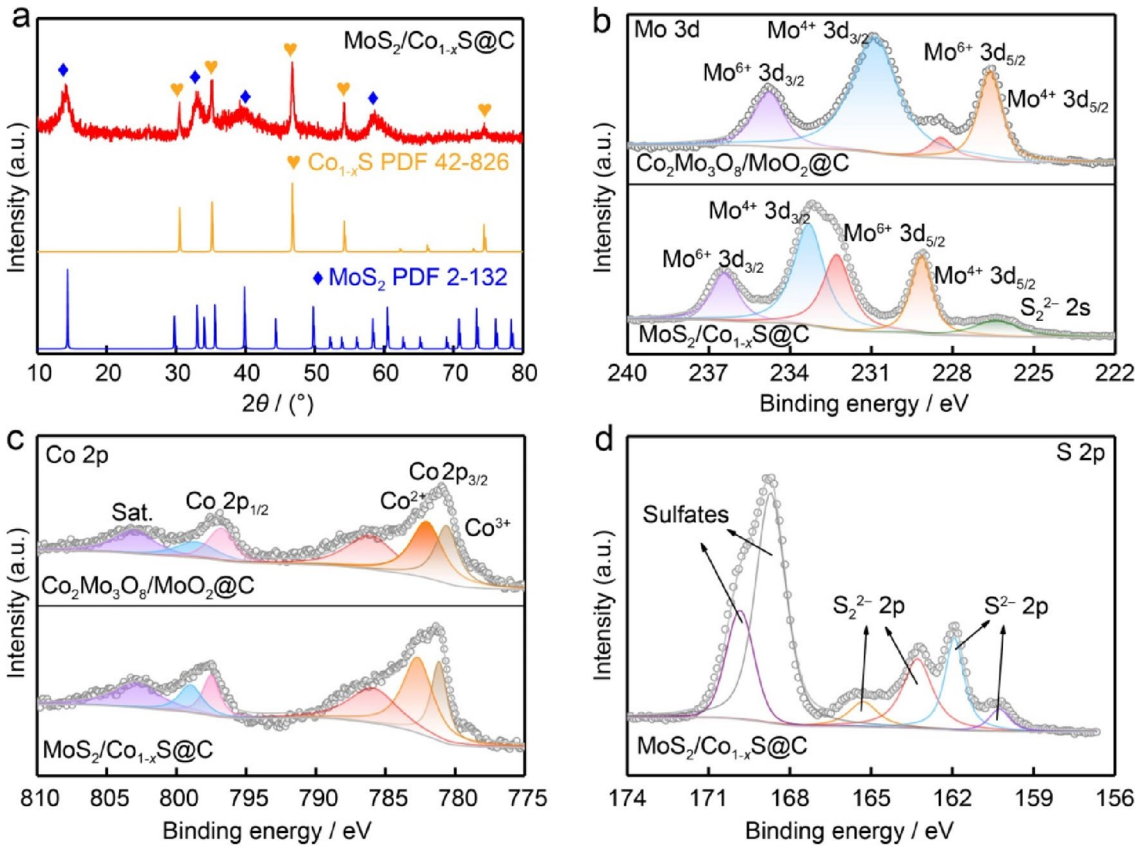

Fig. 2 **a** XRD patterns of the electro-catalysts, High-resolution XPS spectra of $MoS_2/Co_{1-x}S@C$ and $Co_2Mo_3O_8/MoO_2@C$, **b** Mo 3d, **c** Co 2p and **d** S 2p of $MoS_2/Co_{1-x}S@C$

curve in alkaline electrolyte, calibrated by the iR compensation using the corresponding solution resistances (R_s) of all electrodes. It can be seen from Fig. S5a in Supporting Information that $MoS_2/Co_{1-x}S@C$ exhibits relatively excellent performance, and its over-potential is much lower than that of $Co_2Mo_3O_8/MoO_2@C$ and commercial RuO_2 electro-catalysts, which is also lower than those of samples with other concentrations of ion adsorption (Fig. S5b). At the same time, it can be seen from Fig. S6 in Supporting Information that after the OER cycling, the small nanoparticles of different sizes originally loaded on the surface of carbon matrix derived from the filter paper became larger nanoparticles or even nanospheres and nano-blocks. The Tafel slope of $MoS_2/Co_{1-x}S@C$ is 85.4 mV·dec^{-1}, which is significantly smaller than that of $Co_2Mo_3O_8/MoO_2@C$ (98.1 mV·dec^{-1}), RuO_2 (116.2 mV·dec^{-1}), and samples with other concentrations of ion adsorption (Fig. S7a), indicating the enhanced OER kinetics of $MoS_2/Co_{1-x}S@C$ (Fig. 3b). To further reveal the intrinsic catalytic activity of the as-prepared electro-catalysts, the kinetics of the electro-catalysts were further evaluated by EIS, which can reflect the charge transfer ability, as shown in Fig. S7b. At the same time, the fitting results of the equivalent circuit model show that sulfide has a fast charge transfer process (Fig. S8 and Table S1) [51, 52]. The Nyquist plot shows that $MoS_2/Co_{1-x}S@C$ has the smallest resistance to charge transfer, implying optimal mass and charge transfer kinetics and the lowest reaction barrier. This small charge transfer resistance is ascribed to the abundant exposed active sites between the interface of MoS_2 and $Co_{1-x}S$, which is favorable for the charge transfer process. Furthermore, the electrochemically active surface area (ECSA) was further tested and the double layer capacitance (C_{dl}) was calculated. It is observed that $MoS_2/Co_{1-x}S@C$ possesses higher ECSA value (Fig. S9). Figure 3c shows the *V–t* test curve of $MoS_2/Co_{1-x}S@C$ electro-catalyst at 10 mA·cm^{-2}. It could be seen that after 30 h of continuous operation, the potential of $MoS_2/Co_{1-x}S@C$ has a negligible increase, indicating the superior OER durability.

LSV plots showed a standard HER activity of 20% Pt/C as a catalyst benchmarking (Fig. 3d), indicating the normalization of our testing process. Nonetheless, it can be seen that $MoS_2/Co_{1-x}S@C$ exhibits high electrochemical activity than $Co_2Mo_3O_8/MoO_2@C$. The HER over-potential of $MoS_2/Co_{1-x}S@C$ is 135 mV when the current density is 10 mA·cm^{-2}, which is significantly lower than that of $Co_2Mo_3O_8/MoO_2@C$ (217 mV). The hydrogen evolution

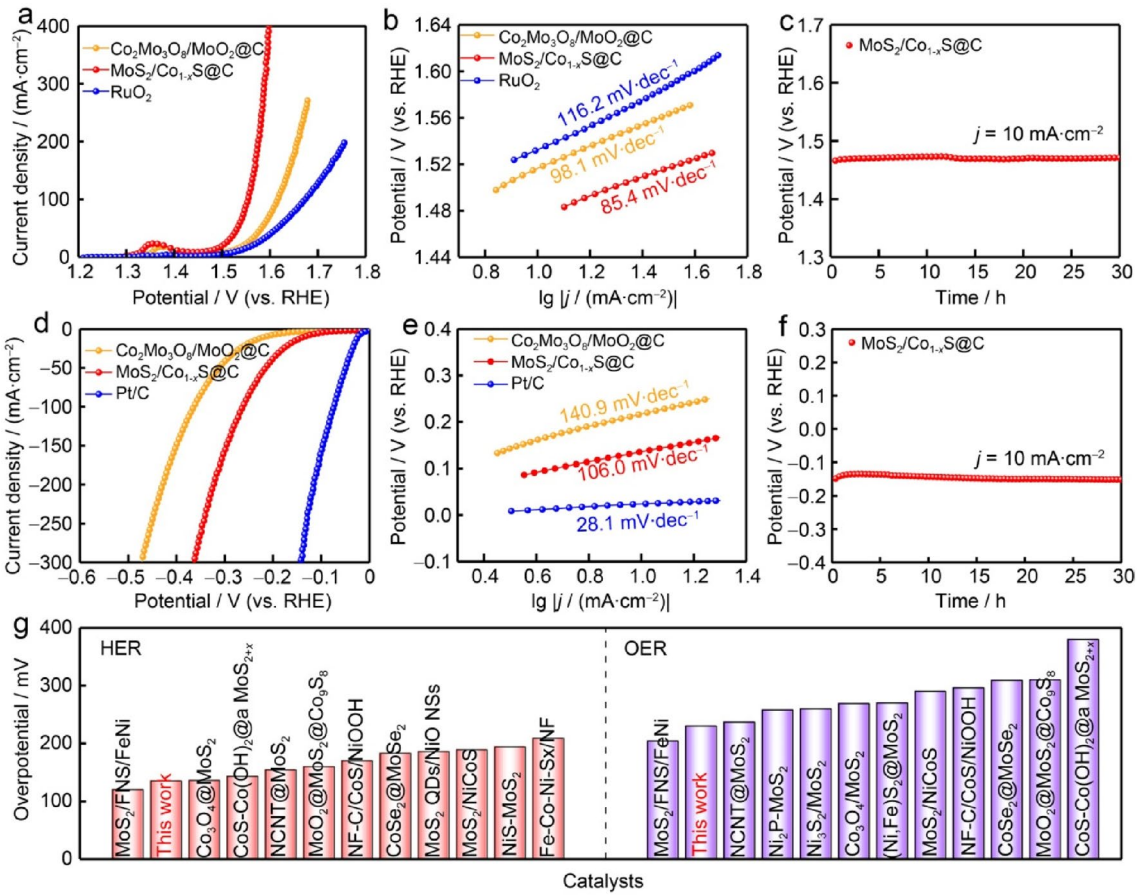

Fig. 3 **a** OER LSV polarization curves and **b** corresponding Tafel plots in 1.0 mol·L^{-1} KOH electrolyte of $MoS_2/Co_{1-x}S$@C, $Co_2Mo_3O_8/MoO_2$@C, and commercial RuO_2. **c** OER Chronopotentiometry curve of $MoS_2/Co_{1-x}S$@C at 10 mA·cm^{-2}. **d** HER LSV polarization curves and **e** corresponding Tafel plots in 1.0 mol·L^{-1} KOH electrolyte for $MoS_2/Co_{1-x}S$@C, $Co_2Mo_3O_8/MoO_2$@C, and commercial Pt/C. **f** HER Chronopotentiometry curve of $MoS_2/Co_{1-x}S$@C at 10 mA·cm^{-2}. **g** Comparison of the HER and OER over-potentials at 10 mA·cm^{-2} for $MoS_2/Co_{1-x}S$@C with previously reported catalysts

performance showed that the sulfurization had a positive effect on the improvement of the electro-catalyst performance. Specifically, sulfide has better catalytic activity and conductivity than oxide. This may be due to the electronic interaction within the $MoS_2/Co_{1-x}S$@C hetero-structures that modulate the optimal HER activity. After HER cycling, the surface morphology of the catalyst was partially agglomerated from the small nanoparticles originally supported on the surface of the carbon matrix (Fig. S10), which may be due to the reduction reaction that occurred during the HER process, and the sulfide was reduced into other reduced cobalt-based and molybdenum-based species. Correspondingly, the catalytic kinetics and mechanism of electro-catalysts were studied by the Tafel slope, which can be used to infer the basic reaction steps. As shown in the Fig. 3e, the Tafel slopes of $Co_2Mo_3O_8/MoO_2$@C, $MoS_2/Co_{1-x}S$@C, and Pt/C were found to be 140.9, 106.0, and 28.1 mV dec^{-1} by fitting, respectively, indicating that the heterojunction formed by MoS_2 and $Co_{1-x}S$ leads to a higher HER reaction rates and kinetics. It is also observed that $MoS_2/Co_{1-x}S$@C at 0.5 mmol·L^{-1} possesses the best HER activity. At the same time, $MoS_2/Co_{1-x}S$@C at 0.5 mmol·L^{-1} concentration shows a smaller Tafel slope compared with other samples, indicating the optimization of the electronic structure and HER dynamics (Fig. S11) $MoS_2/Co_{1-x}S$@C also exhibits excellent HER and OER activity, even eliminating the effect of loading by mass normalization (Fig. S12). Figure 3f shows that $MoS_2/Co_{1-x}S$@C has excellent catalytic durability with negligible decay after 30 h of HER reaction. Importantly, the normalized OER/HER LSV curve of electrochemical surface area (ECSA) still shows excellent intrinsic activity of the $MoS_2/Co_{1-x}S$@C. (Fig. S13) [53]. It is worth noting that $MoS_2/Co_{1-x}S$@C is also an efficient bifunctional electro-catalyst compared to previously reported doped catalysts (Fig. 3g). The above analysis shows that the heterojunction after sulfide makes the catalyst rich in active sites and enhance in electron transport, the charge

transfer resistance is reduced and the catalytic activity is synergistically optimized.

Encouraged by the above results, the as-prepared MoS_2/$Co_{1-x}S$@C was simultaneously used as a free-standing cathode and anode to evaluate the activity of water splitting. The polarization curve in Fig. 4a shows that MoS_2/$Co_{1-x}S$@C has high bifunctional electro-catalytic activity for water splitting. It can be observed from Fig. 4b that MoS_2/$Co_{1-x}S$@C provides 10 mA·cm^{-2} at a cell voltage of 1.60 V, while the combined system of Pt/C and RuO_2 requires a voltage of 1.58 V and $Co_2Mo_3O_8$/MoO_2@C requires 1.75 V, which is much higher than that of MoS_2/$Co_{1-x}S$@C. Besides the high catalytic activity, the catalytic durability of MoS_2/$Co_{1-x}S$@C was also investigated. As shown in Fig. 4c, MoS_2/$Co_{1-x}S$@C exhibits excellent electrochemical stability with negligible loss of overall water splitting performance after continuous operation for 15 h. MoS_2/$Co_{1-x}S$@C still exhibits good stability at large current densities (Fig. S14 and Table S2). Moreover, schematic diagram of the mechanism of the overall water splitting process of MoS_2/$Co_{1-x}S$@C under alkaline conditions is exhibited in Fig. 4d. The formation of heterojunction accelerates the charge transfer at the interface. And the slope of Mott–Schottky curve of sulfide heterojunction is greater than that of oxide precursor, which indicates that sulfide heterojunction can provide faster electron conduction in the electrochemical process, so as to achieve efficient electro-catalytic reaction (Fig. S15). MoS_2/$Co_{1-x}S$@C hetero-structured nano-sheet possesses a larger active surface area, which is conducive to the contact between the electrode and the electrolyte and promotes the mass transfer process. At the same time, carbon derived from the filter paper is used as matrix to ensure full exposure of active sites and improve catalytic stability. Furthermore, the higher degree of graphitization can adjust the electronic transport capacity, so as to obtain admirable conductivity.

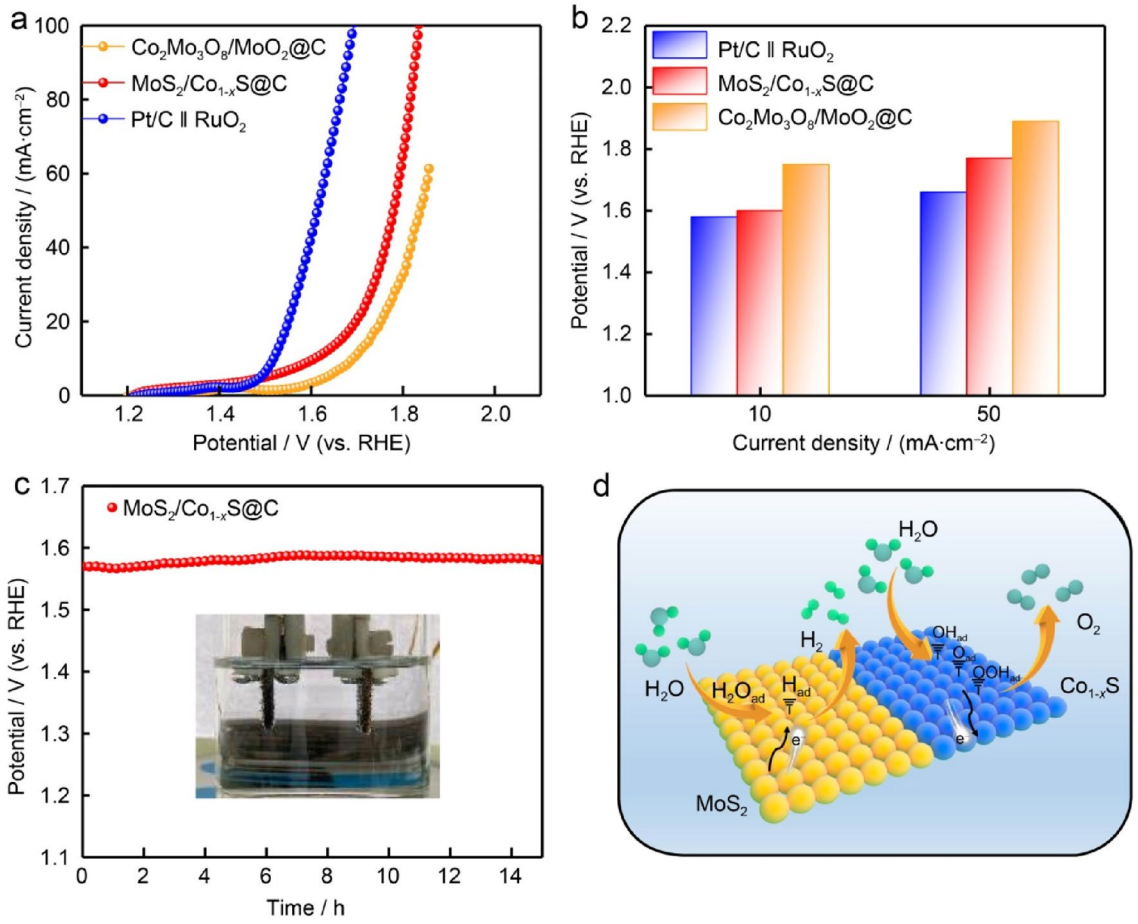

Fig. 4 **a** Water splitting LSV polarization curves of MoS_2/$Co_{1-x}S$@C, $Co_2Mo_3O_8$/MoO_2@C, and commercial RuO_2 ‖ Pt/C. **b** Overpotential comparison of MoS_2/$Co_{1-x}S$@C, $Co_2Mo_3O_8$/MoO_2@C and commercial RuO_2 ‖ Pt/C at 10 mA·cm^{-2} and 50 mA·cm^{-2}. **c** Water splitting Chronopotentiometry curve of MoS_2/Co_{1-x}@C at 10 mA·cm^{-2}. **d** Schematic diagram of the mechanism of water splitting

4 Conclusion

In this work, the $MoS_2/Co_{1-x}S$@C electro-catalyst was successfully fabricated by a simple adsorption–thermal treatment synthesis strategy for the overall water splitting. The sulfide heterojunction electro-catalyst improves the electrochemical performance due to the ultrathin nano-sheet structure. The large specific surface area of the filter paper is conducive to the precipitation and penetration of gas. In addition, the filter paper is used as a sacrificial carrier to provide a carbon source, which improves the conductivity and robustness of the catalyst. More importantly, the hetero-interface formed between MoS_2 and $Co_{1-x}S$ optimizes the electron arrangement on the catalyst surface, and the strong electronic coupling significantly improves the interfacial reactivity. The potential of $MoS_2/Co_{1-x}S$@C for total water splitting is only 1.6 V, and this electro-catalyst also exhibits long-term stability. This study provides a new idea for preparing bifunctional electro-catalysts free of rare metals from cheap and natural environmentally friendly materials.

Supplementary Information The online version contains supplementary material available at https://doi.org/10.1007/s42864-023-00212-6.

Acknowledgements This work was supported by the National Natural Science Foundation of China (51871119, 22075141, and 22101132), Scientific and Technological Innovation Special Fund for Carbon Peak and Carbon Neutrality of Jiangsu Province (BK20220039), Jiangsu Provincial Founds for Natural Science Foundation (BK20180015 and BK20210311), China Postdoctoral Science Foundation (2021M691561 and 2021T140319), Jiangsu Postdoctoral Research Fund (2021K547C) and the Fundamental Research Funds for the Central Universities (kfjj20180605).

Data availability statement The data that support the findings of this study are available from the corresponding authors upon reasonable request.

Declarations

Conflict of interest The authors declare no conflict of interest.

References

1. Huang J, Sheng H, Ross RD, Han J, Wang X, Song B, Jin S. Modifying redox properties and local bonding of Co_3O_4 by CeO_2 enhances oxygen evolution catalysis in acid. Nat Commun. 2021;12(1):3036.
2. Huo WY, Wang SQ, Zhu WH, Zhang ZL, Fang F, Xie ZH, Jiang JQ. Recent progress on high-entropy materials for electrocatalytic water splitting applications. Tungsten. 2021;3(2):161.
3. Song Y, Ji K, Duan H, Shao M. Hydrogen production coupled with water and organic oxidation based on layered double hydroxides. Exploration. 2021;1(3):20210050.
4. Luo M, Liu S, Zhu W, Ye G, Wang J, He Z. An electrodeposited MoS_2-MoO_3−x/Ni_3S_2 heterostructure electrocatalyst for efficient alkaline hydrogen evolution. Chem Eng J. 2022;428: 131055.
5. Dai L, Chen ZN, Li L, Yin P, Liu Z, Zhang H. Ultrathin Ni(0)-embedded $Ni(OH)_2$ heterostructured nanosheets with enhanced electrochemical overall water splitting. Adv Mater. 2020;32(8):1906915.
6. Jin H, Guo C, Liu X, Liu J, Vasileff A, Jiao Y, Zheng Y, Qiao SZ. Emerging two-dimensional nanomaterials for electrocatalysis. Chem Rev. 2018;118(13):6337.
7. Wu Y, Li F, Chen W, Xiang Q, Ma Y, Zhu H, Tao P, Song C, Shang W, Deng T, Wu J. Coupling interface constructions of $MoS_2/Fe_5Ni_4S_8$ heterostructures for efficient electrochemical water splitting. Adv Mater. 2018;30(38):1803151.
8. Qin C, Fan A, Zhang X, Wang S, Yuan X, Dai X. Interface engineering: few-layer MoS_2 coupled to a NiCo-sulfide nanosheet heterostructure as a bifunctional electrocatalyst for overall water splitting. J Mater Chem A. 2019;7(48):27594.
9. Hu F, Yu D, Ye M, Wang H, Hao Y, Wang L, Li L, Han X, Peng S. Lattice-matching formed mesoporous transition metal oxide heterostructures advance water splitting by active Fe–O–Cu bridges. Adv Energy Mater. 2022;12(19):2200067.
10. Xi W, Ren Z, Kong L, Wu J, Du S, Zhu J, Xue Y, Meng H, Fu H. Dual-valence nickel nanosheets covered with thin carbon as bifunctional electrocatalysts for full water splitting. J Mater Chem A. 2016;4(19):7297.
11. Shit S, Chhetri S, Jang W, Murmu NC, Koo H, Samanta P, Kuila T. Cobalt sulfide/nickel sulfide heterostructure directly grown on nickel foam: an efficient and durable electrocatalyst for overall water splitting application. ACS Appl Mater Interfaces. 2018;10(33):27712.
12. Niu Y, Gong S, Liu X, Xu C, Xu M, Sun S-G, Chen Z. Engineering iron-group bimetallic nanotubes as efficient bifunctional oxygen electrocatalysts for flexible Zn–air batteries. eScience. 2022;2(5):546.
13. Xin Y, Kan X, Gan LY, Zhang Z. Heterogeneous bimetallic phosphide/sulfide nanocomposite for efficient solar-energy-driven overall water splitting. ACS Nano. 2017;11(10):10303.
14. Zhang W, Han N, Luo J, Han X, Feng S, Guo W, Xie S, Zhou Z, Subramanian P, Wan K, Arbiol J, Zhang C, Liu S, Xu M, Zhang X, Fransaer J. Critical role of phosphorus in hollow structures cobalt-based phosphides as bifunctional catalysts for water splitting. Small. 2022;18(4):2103561.
15. Chen D, Lu R, Pu Z, Zhu J, Li H-W, Liu F, Hu S, Luo X, Wu J, Zhao Y, Mu S. Ru-doped 3D flower-like bimetallic phosphide with a climbing effect on overall water splitting. Appl Catal B: Environ. 2020;279: 119396.
16. Guo X, Wan X, Liu Q, Li Y, Li W, Shui J. Phosphated IrMo bimetallic cluster for efficient hydrogen evolution reaction. eScience. 2022;2(3):304.
17. Li L, Yu D, Li P, Huang H, Xie D, Lin CC, Hu F, Chen HY, Peng S. Interfacial electronic coupling of ultrathin transition-metal hydroxide nanosheets with layered MXenes as a new prototype for platinum-like hydrogen evolution. Energy Environ Sci. 2021;14(12):6419.
18. Jiao C, Bo X, Zhou M. Electrocatalytic water splitting at nitrogen-doped carbon layers-encapsulated nickel cobalt selenide. J Energy Chem. 2019;34:161.
19. Deng L, Hu F, Ma M, Huang SC, Xiong Y, Chen HY, Li L, Peng S. Electronic modulation caused by interfacial Ni–O–M (M = Ru, Ir, Pd) bonding for accelerating hydrogen evolution kinetics. Angew Chem Int Ed. 2021;60(41):22276.
20. Zhou YN, Zhu YR, Chen XY, Dong B, Li QZ, Chai YM. Carbon–based transition metal sulfides/selenides nanostructures for electrocatalytic water splitting. J Alloys Compd. 2021;852: 156810.
21. Guo Y, Park T, Yi JW, Henzie J, Kim J, Wang Z, Jiang B, Bando Y, Sugahara Y, Tang J, Yamauchi Y. Nanoarchitectonics for transition-metal-sulfide-based electrocatalysts for water splitting. Adv Mater. 2019;31(17):1807134.
22. Wang M, Zhang L, He Y, Zhu H. Recent advances in transition-metal-sulfide-based bifunctional electrocatalysts for overall water splitting. J Mater Chem A. 2021;9(9):5320.

23. Xiong Q, Wang Y, Liu PF, Zheng LR, Wang G, Yang HG, Wong PK, Zhang H, Zhao H. Cobalt covalent doping in MoS_2 to induce bifunctionality of overall water splitting. Adv Mater. 2018;30:1801450.
24. Zhang J, Wang T, Pohl D, Rellinghaus B, Dong R, Liu S, Zhuang X, Feng X. Interface engineering of MoS_2/Ni_3S_2 heterostructures for highly enhanced electrochemical overall-water-splitting activity. Angew Chem Int Ed. 2016;55(23):6702.
25. Li Z, Hu M, Wang P, Liu J, Yao J, Li C. Heterojunction catalyst in electrocatalytic water splitting. Coord Chem Rev. 2021;439: 213953.
26. Xiong P, Zhang X, Wan H, Wang S, Zhao Y, Zhang J, Zhou D, Gao W, Ma R, Sasaki T, Wang G. Interface modulation of two-dimensional superlattices for efficient overall water splitting. Nano Lett. 2019;19(7):4518.
27. Jiao J, Yang W, Pan Y, Zhang C, Liu S, Chen C, Wang D. Interface engineering of partially phosphidated Co@Co-P@NPCNTs for highly enhanced electrochemical overall water splitting. Small. 2020;16(41):2002124.
28. Wang W, Dong J, Ye X, Li Y, Ma Y, Qi L. Heterostructured TiO_2 nanorod@nanobowl arrays for efficient photoelectrochemical water splitting. Small. 2016;12(11):1469.
29. Zhang J, Zhang Q, Feng X. Support and interface effects in water-splitting electrocatalysts. Adv Mater. 2019;31(31):1808167.
30. Li Y, Yin J, An L, Lu M, Sun K, Zhao YQ, Gao D, Cheng F, Xi P. FeS_2/CoS_2 Interface nanosheets as efficient bifunctional electrocatalyst for overall water splitting. Small. 2018;14(26):1801070.
31. Shit S, Bolar S, Murmu NC, Kuila T. Tailoring the bifunctional electrocatalytic activity of electrodeposited molybdenum sulfide/iron oxide heterostructure to achieve excellent overall water splitting. Chem Eng J. 2021;417: 129333.
32. Liu J, Wang J, Zhang B, Ruan Y, Wan H, Ji X, Xu K, Zha D, Miao L, Jiang J. Mutually beneficial $Co_3O_4@MoS_2$ heterostructures as a highly efficient bifunctional catalyst for electrochemical overall water splitting. J Mater Chem A. 2018;6(5):2067.
33. Wang L, Hao Y, Deng L, Hu F, Zhao S, Li L, Peng S. Rapid complete reconfiguration induced actual active species for industrial hydrogen evolution reaction. Nat Commun. 2022;13(1):5785.
34. Aftab U, Tahira A, Mazzaro R, Morandi V, Abro MI, Baloch MM, Syed JA, Nafady A, Ibupoto ZH. Facile $NiCo_2S_4$/C nanocomposite: an efficient material for water oxidation. Tungsten. 2020;2(4):403.
35. An K, Zheng Y, Xu X, Wang Y. Filter paper derived three-dimensional mesoporous carbon with Co_3O_4 loaded on surface: an excellent binder-free air-cathode for rechargeable Zinc-air battery. J Solid State Chem. 2019;270:539.
36. Xu B, Chen Z, Yang X, Wang X, Huang Y, Li C. Electronic modulation of carbon-encapsulated NiSe composites via Fe doping for synergistic oxygen evolution. Chem Commun. 2018;54(65):9075.
37. Wang W, Wang Z, Hu Y, Liu Y, Chen S. A potential-driven switch of activity promotion mode for the oxygen evolution reaction at Co_3O_4/NiO_xH_y interface. eScience. 2022;2(4):438.
38. Li Y, Liu Y, Xing D, Wang J, Zheng L, Wang Z, Wang P, Zheng Z, Cheng H, Dai Y, Huang B. 2D/2D heterostructure of ultrathin $BiVO_4/Ti_3C_2$ nanosheets for photocatalytic overall Water splitting. Appl Catal B: Environ. 2021;285: 119855.
39. Wang J, Du CF, Xue Y, Tan X, Kang J, Gao Y, Yu H, Yan Q. MXenes as a versatile platform for reactive surface modification and superior sodium-ion storages. Exploration. 2021;1(2):20210024.
40. Li Q, Li L, Yu X, Wu X, Xie Z, Wang X, Lu Z, Zhang X, Huang Y, Yang X. Ultrafine platinum particles anchored on porous boron nitride enabling excellent stability and activity for oxygen reduction reaction. Chem Eng J. 2020;399: 125827.
41. Wang L, Yu H, Zhao S, Ma H, Li L, Hu F, Li L, Pan H, El-Khatib KM, Peng S. Electronic modulation of cobalt–molybdenum oxide via Te doping embedded in a carbon matrix for superior overall water splitting. Inorg Chem Front. 2022;9(15):3788.
42. Pan ZY, Tang Z, Zhan YZ, Sun D. Three-dimensional porous $CoNiO_2$@reduced graphene oxide nanosheet arrays/nickel foam as a highly efficient bifunctional electrocatalyst for overall water splitting. Tungsten. 2020;2(4):390.
43. Babar P, Patil K, Mahmood J, Kim S-J, Kim JH, Yavuz CT. Low-overpotential overall water splitting by a cooperative interface of cobalt-iron hydroxide and iron oxyhydroxide. Cell Rep Phys Sci. 2022;3(2):100762.
44. Yin D, Cao YD, Chai DF, Fan LL, Gao GG, Wang ML, Liu H, Kang Z. A WO*x* mediated interface boosts the activity and stability of Pt-catalyst for alkaline water splitting. Chem Eng J. 2022;431: 133287.
45. Yu D, Ma Y, Hu F, Lin CC, Li L, Chen HY, Han X, Peng S. Dual-sites coordination engineering of single atom catalysts for flexible metal–air batteries. Adv Energy Mater. 2021;11(30):2101242.
46. Wang A, Cheng L, Shen X, Chen X, Zhu W, Zhao W, Lv C. Porphyrin coordination polymer/$Co_{1-x}S$ composite electrocatalyst for efficient oxygen evolution reaction. Chem Eng J. 2020;400: 125975.
47. Xue Y, Min S, Meng J, Liu X, Lei Y, Tian L, Wang F. Light-induced confined growth of amorphous Co doped MoS_x nanodots on TiO_2 nanoparticles for efficient and stable in situ photocatalytic H_2 evolution. Int J Hydrog Energy. 2019;44(16):8133.
48. Liu R, Fei HL, Ye GL. Recent advances in single metal atom-doped MoS_2 as catalysts for hydrogen evolution reaction. Tungsten. 2020;2(2):147.
49. Li XX, Liu XC, Liu C, Zeng JM, Qi XP. Co_3O_4/stainless steel catalyst with synergistic effect of oxygen vacancies and phosphorus doping for overall water splitting. Tungsten. 2023;5:100.
50. Shit S, Bolar S, Murmu NC, Kuila T. Minimal lanthanum-doping triggered enhancement in bifunctional water splitting activity of molybdenum oxide/sulfide heterostructure through structural evolution. Chem Eng J. 2022;428: 131131.
51. Han WK, Wei JX, Xiao K, Ouyang T, Peng X, Zhao S, Liu ZQ. Activating lattice oxygen in layered lithium oxides through cation vacancies for enhanced urea electrolysis. Angew Chem Int Ed. 2022;61:202206050.
52. Wei JX, Xiao K, Chen YX, Guo XP, Huang B, Liu ZQ. In-situ precise anchoring of Pt single atoms in spinel Mn_3O_4 for a highly efficient hydrogen evolution reaction. Energy Environ Sci. 2022;15:4592.
53. Xiao K, Lin RT, Wei JX, Li N, Li H, Ma T, Liu ZQ. Electrochemical disproportionation strategy to in-situ fill cation vacancies with Ru single atoms. Nano Res. 2022;15:4980.